1 **Title: Phytoplankton traits from long-term oceanographic time-series**

2 Running page head: Phytoplankton traits from time-series data

3

4 Crispin M Mutshinda[1], Zoe V Finkel[2], Claire E Widdicombe[3], Andrew J Irwin[1]

5 [1] Mathematics & Computer Science, Mount Allison University, Sackville, NB, Canada, E4L

6 1E6

7 [2] Environmental Science, Mount Allison University, Sackville, NB, Canada, E4L 1A7

8 [3] Plymouth Marine Laboratory, Prospect Place, Plymouth, UK, PL1 3DH

9

11

12 **Abstract**

13 Phytoplankton trait-based modeling is a mechanistic approach to describing species and

14 community dynamics in ecosystem models. Trait values are usually extracted from

15 laboratory studies of single species, which presents challenges for understanding the

16 immense diversity of phytoplankton species and the wide range of dynamic ocean

17 environments. Here we use a Bayesian approach and a trait-based model to extract traits

18 for four functional types and ten diatom species from field data collected at Station L4 in

19 the Western Channel Observatory. We find differences in maximum net growth rate,

20 temperature optimum and sensitivity, half-saturation constants for light and nitrogen, and

21 density-dependent loss terms across the functional types. We find evidence of very high

22 linear loss rates, suggesting that grazing may be even more important than commonly

23 assumed and differences in density-dependent loss rates across functional types, indicating

24 the presence of strong niche differentiation among functional types. Very low half-

25 saturation constants for nitrogen at the functional type level may indicate widespread

26 mixotrophy. At the species level, we find a wide range of density-dependent effects, which

27 may be a signal of diversity in grazing susceptibility or biotic interactions. This approach

28 may be a way to obtain more realistic and better-constrained trait-values for functional

29 types to be used in ecosystem modeling.

30

Introduction

Phytoplankton perform about half of global photosynthesis, form the base of the marine food web and are an important driver of biogeochemical cycles (Field et al. 1998). Model projections of changes in phytoplankton primary production with climate over the next century are extremely variable (Finkel et al. 2010, Finkel 2014). Projections of changes in communities and biogeochemical cycling usually depend on mechanistic models of phytoplankton productivity parameterized with traits of phytoplankton species (Le Quéré et al. 2005, Litchman et al. 2006). The traits used in models vary according to the research questions, but most commonly include maximum growth rate, Arrhenius-like temperature effects on growth rate, half-saturation parameters linking the growth rate to resource availability, and grazing susceptibility (Litchman et al. 2007, Irwin & Finkel 2016). At present, many of these parameters are not well constrained for phytoplankton communities (Anderson 2005, Irwin & Finkel 2016).

Phytoplankton are evolutionarily and ecologically diverse and include many phyla and tens of thousands of species (Sournia et al. 1991, de Vargas et al. 2015). This complexity presents several challenges for trait-based modeling. Trait values measured in the lab are almost always determined for a few key species, while their application in models of natural communities usually apply to dozens to thousands of species. The aggregation of similar species into biogeochemically defined functional types greatly simplifies models, but there is no clear way to decide which species should be used as representatives of each functional type (Merico et al. 2004, Le Quéré et al. 2005, Hood et al. 2006). Trait values for species in the same functional type and trait values used in models vary widely, commonly by a factor of 10-100 (Anderson 2005, Irwin & Finkel 2016). It is not clear how to average trait values across species to represent a functional type since phytoplankton growth rate is a non-linear function of trait values. Furthermore, species well adapted to lab conditions may not be representative of their respective functional types growing in natural communities. A second set of challenges concerns the difficulty of using lab-based estimates of trait values in a field context. Trait values quantified using laboratory cultures under controlled conditions are stable under repeated measurement, but there is a challenge in identifying the most appropriate conditions for culture experiments. For example, the maximum growth rate is commonly estimated in the lab, but

62   differences in culture conditions from one lab to another means there is always some doubt

63   about the true maximum growth rate for a species (Boyd et al. 2013). Trait-values,

64   including maximum growth rate and nutrient uptake rates, estimated in the field can differ

65   substantially from those measured in the lab (Furnas 1991, Laws 2013, Lomas et al. 2014).

66   Cultures grown under equilibrium conditions in the lab may not reveal key acclimation

67   traits or the consequences of environmental variability that can be crucial to the fate of

68   phytoplankton in natural communities (Grover 1991, Raven 2011). In summary, trait

69   values for most phytoplankton species are not available and we do not currently have

70   enough data to strongly constrain trait values used in functional type models (Anderson

71   2005, Flynn et al. 2015).

72   An approach that addresses many of these challenges for determining trait values

73   for function types is to estimate those values from long-term time series of natural

74   communities observed in the field. Our goal is to obtain quantitative estimates of trait

75   values that define the dynamics of the biomass of phytoplankton functional types. These

76   trait values will be affected by the species that are present in the community, the range of

77   environmental conditions observed, the spectrum of environmental variability, as well as

78   abiotic and biotic interactions, so we call them realized traits in recognition that they are

79   not the fixed traits of a particular species. This label is an echo of the difference between

80   fundamental and realized niches, where the realized niche is measured in a community and

81   can differ from the fundamental niche (Hutchinson 1957, Colwell & Rangel 2009). Here we

82   obtain realized trait values by fitting a model of biomass dynamics to time series of

83   phytoplankton functional type biomass and coincident environmental conditions. The

84   model describes temporal biomass changes in terms of net growth rate modified by

85   temperature, irradiance, total available nitrogen concentration, and a density dependent

86   loss term. We adopt a hierarchical Bayesian modeling approach and use Markov-chain

87   Monte Carlo (MCMC) methods to simulate from the joint posterior of the model

88   parameters, in particular the traits of interest. Realized trait values estimated from field

89   data may be quite different from trait values obtained in the lab and may vary across

90   communities in different locations. The advantages of these realized traits compared to

91   species-level traits quantified in the lab is that these traits by definition describe observed

92   community dynamics.

93

Methods

Data

      We used data from the Western Channel Observatory (WCO) oceanographic time-series (www.westernchannelobservatory.org.uk) in the Western English Channel. The WCO data include phytoplankton, zooplankton, and fish trawls together with measurements of several physical and chemical environmental parameters such as temperature, salinity and nutrient concentrations. The data used here were collected at Station L4 (50° 15.00′N, 4° 13.02′W) located about 10 km south of the Plymouth breakwater with a water column depth of about 50 m (Harris 2010). We used 349 weekly observations of taxonomically resolved phytoplankton abundance, temperature, nitrate, nitrite, and ammonium concentrations sampled at 10 m depth in the upper mixed layer and sea-surface irradiance collected over a 7-year period spanning 15 April 2003 through 31 December 2009. Average biovolume measurements were recorded for each species (Widdicombe et al. 2010) and converted to carbon content (Menden-Deuer & Lessard 2000) to obtain biomass concentrations (mg C m^{-3}) for each species. We used observations of 193 taxonomic categories identified as 138 species, 27 genera, and 28 size-classes for broader morphological categories. Biomass concentrations were aggregated into four functional types: diatoms, dinoflagellates, coccolithophorids, and phytoflagellates. The phytoflagellate type is taxonomically diverse but is dominated (more than 50% of the biomass) by unidentified flagellates less than 5 μm in diameter. Some species may be benthic or tychoplanktonic. We added together the concentrations of nitrate, nitrite, and ammonium to obtain a single inorganic nitrogen (mg m^{-3}) concentration. Most of the variation in total nitrogen concentration is due to variation in nitrate concentration. Irradiance (mol m^{-2} d^{-1}) was measured continuously above the sea-surface near Station L4 at Plymouth and averaged over the day. Data for missing weeks were imputed by linear interpolation using the na.approx function from the zoo library in R (R Core Team 2016).

The model

      We describe the multiplicative growth rate of each functional type's biomass as the product of the following 5 components: (i) a net growth rate reduced by limitation due to

124   either low light or low nitrogen concentration, (ii) a temperature effect, (iii) a density

125   feedback term dependent on the biomass of the focal functional type, (iv) a density

126   feedback term dependent on the biomass of all phytoplankton not in the focal functional

127   type, and (v) a positive multiplicative noise term. The change in biomass from one week to

128   the next (from week $w-1$ to week w) for each functional type i is modeled by multiplying

129   the biomass in week $w-1$ by the (multiplicative) growth rate according to a stochastic

130   Gompertz model (Saitoh et al. 1997, Mutshinda et al. 2009, Mutshinda et al. 2011). We

131   chose to model the net growth rate as a linear combination of density-independent growth

132   rate and density-dependent losses, which is most appropriate given the lack of direct

133   information about grazing rates, grazer biomass, or viral abundance. Therefore, the

134   biomass concentration $Y_{i,w}$ (in $\mathrm{mg\,C\,m^{-3}}$) of the ith functional type for each week after the

135   first $(w \geq 2)$ is described by

136

137   $$Y_{i,w} = Y_{i,w-1} \exp\{r_{i,w} + \alpha_i \log(Y_{i,w-1}) + \phi_i \log(Z_{i,w-1})\} \eta_{i,w}, \qquad (1)$$

138

139   where $Z_{i,w}$ is the combined biomass concentration of all phytoplankton not including the

140   ith functional type during week w. The growth rate, which appears in the exponent of Eq.

141   (1), is composed of a density-independent component, $r_{i,w}$, and a density-dependent

142   component, $\alpha_i \log(Y_{i,w-1}) + \phi_i \log(Z_{i,w-1})$. Stochastic noise enters the biomass dynamical

143   model (Eq. 1) through the random multiplicative noise $\eta_{i,w} > 0$ that we assume to be serially

144   independent and log-normally distributed with median one and mean $\exp(\sigma_{i,w}^2/2)$, so that

145   the $\log(\eta_{i,w})$ are independently zero-mean normal with respective variances $\sigma_{i,w}^2$. The

146   unstructured stochastic noise term lumps together the variability due to all un-modelled

147   processes: demographic stochasticity, sampling error and the environmental variability

148   attributable to other variables not included in the model. The log-normal distribution is

149   widely used to describe species abundance and biomass patterns (MacArthur 1960,

150   Sugihara 1980) on both theoretical and empirical grounds. We showed that biomass

151   distributions at this site are log-normal in an earlier study (Mutshinda et al. 2016). The

152   notation is summarized in Table 1.

153   The traits to be estimated appear in the growth rate terms. The density-independent

154   component of growth rate, $r_{i,w}$, for functional type i from week w-1 to week w depends on

155   Michaelis-Menten functions of irradiance (PAR, mol m^{-2} d^{-1}) and nitrogen concentration (N,

156   μmol L^{-1}), and a function of temperature (T, °C), according to

157    $$r_{i,w} = \mu_i \min\left(\frac{PAR_{w-1}}{k_{E,i}+PAR_{w-1}}, \frac{N_{w-1}}{k_{N,i}+N_{w-1}}\right) - \beta_i|T_{w-1} - \theta_i| \qquad (2)$$

158   where θ_i denotes the optimum growth temperature for the biomass of functional type i

159   and $\beta_i > 0$ is a temperature sensitivity parameter intended to quantify the increase in the

160   density-independent growth rate $r_{i,w}$ for a 1°C change in temperature towards the

161   optimum temperature θ_i and *vice-versa*. The optimal temperatures θ_i for growth of each

162   functional type are assigned priors and estimated from the data within our Bayesian

163   framework. Saturating functions of irradiance and nitrogen concentration and their

164   combination with a minimum function are commonly used to moderate growth rate

165   (Denman & Peña 1999, Healey et al. 2009). The net growth rate $\mu_i > 0$ is the density-

166   independent growth rate of the ith functional type at optimal temperature, irradiance and

167   nitrogen concentration. The effects of irradiance and nitrogen concentration on the growth

168   rate are represented by saturating functions parameterized by the half-saturation

169   constants $k_{E,i} > 0$ and $k_{N,i} > 0$ which are respectively the irradiance level and nitrogen

170   concentration at which the net growth rate at optimal temperature drops to $\mu_i/2$. The

171   Michaelis-Menten saturating functions are combined with a minimum function so that only

172   the most limiting resource affects growth rate at a time, according to Liebig's law of the

173   minimum (van der Ploeg & Kirkham 1999). During model development, we explored the

174   possibility of a multiplicative interaction between light and nutrients, but found the results

175   to be more difficult to interpret.

176   To accommodate density-dependent factors including grazing, viral attack,

177   aggregation and sinking, we introduce density dependent loss terms. In the absence of

178   direct observations of these losses, we parameterize the density-dependent losses with α_i

179   and ϕ_i to quantify the feedbacks on the growth rate of the ith functional type from its own

180   biomass and from the combined biomass of the other functional types in the community,

181   respectively. The terms involving α_i and ϕ_i distinguish two different density-dependent

182   loss terms, which could result from specialist and generalist grazer populations. For the

183   purposes of estimating the parameters in the model, we rewrote Eq. (1) on the natural

184   logarithmic scale as

185     $$y_w = y_{w-1} + \mu_i \min\left(\frac{PAR_{w-1}}{k_{E,i}+PAR_{w-1}}, \frac{N_{w-1}}{k_{N,i}+N_{w-1}}\right) - \beta_i|T_{w-1} - \theta_i| + \alpha_i y_{i,w-1} + \phi_i z_{i,w-1} + \varepsilon_{i,w}$$

186   (3)

187   where $y_{i,w} = \log(Y_{i,w})$, $z_{i,w} = \log(Z_{i,w})$ and $\varepsilon_{i,w} = \log(\eta_{i,w}) \sim N(0, \sigma^2_{i,w})$.

188   We adapted the functional-type level model described above to define traits at the

189   species level. This task was challenging for two reasons: the greatly increased number of

190   parameters to be estimated and the fact that most species are absent from the time series

191   for most of the time, either because they were absent or their abundance was below the

192   detection limit. By contrast, missing values were rare in the time series of functional type

193   biomasses. We restricted the species-level analysis to the 10 diatoms that were observed in

194   about half of the sampling occasions or more. These species may not be representative of

195   the functional type dynamics as a whole because the selected species only represent 11%

196   of the diatom functional type biomass. In order to estimate a growth rate, biomass

197   observations for any particular species must be available on numerous pairs of successive

198   weeks. We extracted pairs of observations from the full time series to estimate the growth

199   rate from week *w-1* to *w*, conditioned on the species being observed during week *w-1*. The

200   species-level model differed from Eqns. (1-3) only in the definition of the biomass terms

201     $Y_{i,w}$ and $Z_{i,w}$ and the interpretation of the density-dependent terms α and ϕ. To emphasize

202   the differences between the functional type and species-level models, we have added a

203   superscript *S* to the notation for each trait in the species-level model. In the species model,

204     $Y_{i,w}$ was the biomass of species i in week *w*, and $Z_{i,w}$ was the sum of the biomass of all

205   species in the same functional type as species i except for species i in week *w*. The density-

206   dependent parameter α reflected the effect of species i on itself while ϕ described the

207 density-dependent loss due to all species in the same functional type as species *i* except for

208 species *i*.

209   The model was developed and fit to the data with a Bayesian approach (Gelman et

210 al. 2013). Bayesian inference is an approach to statistical inference where all unknown

211 quantities are considered as random variables. The uncertainty about plausible values of

212 an unknown quantity θ before the data is taken into consideration is represented by a

213 probability distribution $p(\theta)$ called the prior distribution. Upon observing the data, the

214 prior distribution is combined with the likelihood function (the sampling distribution of

215 the data) $p(y|\theta)$ through Bayes' rule to produce a posterior distribution $p(\theta|y)$

216 $$p(\theta|y) = \frac{p(y|\theta)p(\theta)}{p(y)},$$ (4)

217

218 where $p(y) = \int_{\Theta} p(y|\theta)p(\theta)d\theta$ is the marginal distribution of the data which is the

219 normalizing constant making $p(\theta|y)$ a proper probability distribution. Therefore, Eq. (4)

220 can be written as

221

222 $$p(\theta|y) \propto p(y|\theta)p(\theta)$$ (5)

223

224 where $\propto$ stands for " proportional to".

225   The posterior distribution represents the data-updated knowledge and forms the

226 basis of Bayesian inference about unknown quantities including model parameters, missing

227 values, and yet unseen data. Having an entire distribution rather than point estimates

228 allows one to fully account for uncertainty. Bayesian conclusions are essentially probability

229 statements based on the posterior distribution. All Bayesian computations are based on

230 probability rules, resulting in more intuitive statements than counterparts in classical

231 statistics.

232   The hierarchical priors in the Bayesian model allowed us to specify a model with

233 many traits for many functional types or taxonomic units without risking over-fitting the

234 data or running into convergence problems that plague other nonlinear optimization

235 methods. The shared hyper-priors effectively pooled data across taxa when there are few

236 data while allowing trait value estimates to be differentiated across taxa when supported

237 by the data. The model fitting to the functional type biomass data was based on the

238 following essentially non-informative prior distributions for the model parameters.

239     $k_{E,i} \sim \mathrm{N}(0,100)\,\mathrm{I}(k_{E,i} > 0)$, where $\mathrm{I}(.)$ denotes the indicator function which takes the value 1

240   when its argument is true and the value 0 otherwise, $k_{N,i} \sim \mathrm{N}(0,10)\,\mathrm{I}(k_{N,i} > 0)$,

241     $\beta_i \sim \mathrm{N}(0,1)\,\mathrm{I}(\beta_i > 0)$, $\theta_i \sim \mathrm{N}(\overline{T},10)$, where $\overline{T}$ is the mean temperature over the study period,

242     $\alpha_i \sim \mathrm{N}(0,1)$, $\phi_i \sim \mathrm{N}(0,1)$, $\sigma_{i,w}^2 \sim \mathrm{InvGamma}(a,b)$, $a \sim \mathrm{Gamma}(1,1)$ and $b \sim \mathrm{Gamma}(1,1)$. We

243   imposed fairly informative $\mathrm{Gamma}(5,5)$ priors independently on the net growth rates μ_i

244   to enforce identifiability. For the species model, the hierarchical priors were designed to

245   provide identical trait estimates for all species if the data did not oppose this possibility.

246   The main problem of Bayesian inference comes from the difficulty in evaluating

247   integrals like the one in the denominator of Eq. (4). In most practical cases the posterior is

248   not available in closed form so sampling-based algorithms, mostly Markov chain Monte

249   Carlo (MCMC) methods (Gilks 1996) are used to simulate from it and base inferences on

250   the simulated sample. Markov chain Monte Carlo methods indirectly simulate from a

251   distribution g when direct simulation from g is difficult or impossible. The rationale of

252   MCMC sampling is to set up a Markov chain whose stationary distribution is the

253   distribution g of interest, in this case the joint posterior distribution $p(\theta \mid y)$. Consequently,

254   simulation of $\theta^{(1)}$, $\theta^{(2)}$,... from the chain yields a series with the property that the marginal

255   density of $\theta^{(j)}$ for large enough j is approximately g. In other words, for a large enough

256   "burn-in" period n, $\theta^{(n+1)}$, $\theta^{(n+2)}$,... can be regarded as a dependent series with marginal

257   density g. Therefore, empirical moments of this series yield approximations of the

258   moments of g.

259   We used Markov chain Monte Carlo (MCMC) simulation (Gilks 2005) implemented

260   in OpenBUGS (Thomas et al. 2006) to sample from the joint posterior of the model

261   parameters. We assessed the convergence of the Markov chains through visual inspection

262   of traceplots and autocorrelation functions. We ran three parallel Markov chains starting

263   from dispersed initial values for 60,000 iterations and discarded the first 30,000 samples

264   from each Markov chain as burn-in. We used the remaining 30,000 samples to generate the

265   posterior distributions on our parameters, retaining every 30th sample to reduce the

266   sample autocorrelation. Our results were robust to changes in the range of priors.

267

Results

269   The three environmental drivers of phytoplankton growth rate included in this

270 study (temperature, irradiance, and nitrogen concentration) exhibit strong, regular

271 seasonal oscillations over the seven-year time series (Widdicombe et al. 2010, Mutshinda

272 et al. 2016). The phytoplankton biomass for each of four functional types each exhibit

273 distinctive patterns of intra-annual variation (Fig. 1). Diatoms bloom first, increasing

274 steadily in biomass from day 60 to day 180. Dinoflagellates and coccolithophorids bloom

275 slightly later, reaching a maximum biomass at approximately day 225. The amplitude of

276 dinoflagellate biomass is the greatest across the four types and their sustained maximum

277 growth and loss rates are also the largest. Phytoflagellates have the least inter-annual

278 variability, with two minor biomass peaks at approximately day 110 and day 215. Our

279 model is able to describe the biomass dynamics, explaining on average between 51% (for

280 diatoms) and 95% (for phytoflagellates) of the variation in the biomass of individual

281 functional types. More importantly, the model produces accurate biomass predictions

282 reflected in narrow, relative to the total variation in the data, posterior predictive intervals

283 (Fig 1). There was insufficient temporal resolution in the data to observe short-term

284 acclimation to changing conditions, so our focus remained on steady-state traits similar to

285 those usually used in phytoplankton community models.

286

287 *Functional-type level analysis*

288   The maximum net growth rate trait, μ_i, is the largest growth rate of functional type

289 i under any irradiance and nutrient conditions, at its optimal temperature for growth, not

290 including density-dependent grazing, but incorporating linear grazing rates. There is

291 substantial variability in the maximum net growth rate between functional types (whiskers

292 on Fig. 2a). As a group, diatoms have the largest net growth rate with median doubling time

293 3.9 days, followed by dinoflagellate with mean doubling time 5.5 days, and phytoflagellate

294 with mean 6.7 days. Coccolithophores have the lowest net growth rate with median

295 doubling time 8.9 days.

296   The estimated optimal temperatures for growth for diatom, dinoflagellate,

297   coccolithophorid, and phytoflagellate biomass are 15°C, 20°C, 19°C and 11°C, respectively,

298   implying that higher temperature conditions would favor dinoflagellate and

299   coccolithophorid biomass accumulation (Fig. 2b). As a group, dinoflagellates are the most

300   responsive to temperature changes with a sensitivity parameter roughly twice as large as

301   those of diatoms and coccolithophorids (Fig. 2c). On the other hand, the phytoflagellate

302   biomass is essentially insensitive to temperature changes at Station L4.

303   The nitrogen (nitrate, nitrite, plus ammonia) half-saturation constants, k_N, for all

304   groups are comparable to those found in lab studies and used in models (Fig. 2d). The

305   phytoflagellates have the smallest half-saturation constants for irradiance, which is

306   consistent with their relatively small amplitude of biomass variation over the time series.

307   The half-saturation constants for irradiance are not credibly different from one another for

308   the other three phytoplankton functional types and exhibit variability of two-fold or more

309   within their 95% credible intervals (Fig. 2e). The half-saturation constants for nitrogen

310   concentration (posterior means ranging from 0.02-0.3 µmol L^{-1}) are quite close to the

311   minimum values of the corresponding environmental data observed over the time-series

312   (0-15 µmol L^{-1}), which suggests that this trait may not be particularly informative for

313   predicting the growth rate of these functional types at this location for most of the year.

314   Conversely, the half-saturating constants for sea-surface irradiance (10-30 mol m^{-2} d^{-1})

315   span most of the lower half of the inter-annual variation in irradiance (10-50 mol m^{-2} d^{-1}),

316   indicating that phytoplankton growth rates vary with irradiance (light is sub-saturating)

317   for much of the year (Fig. 2e).

318   All four phytoplankton functional types are affected by density-dependent loss rates

319   (Fig. 2f). These losses have the largest effect at high biomass concentrations and can

320   explain the maximum biomass concentration for each functional type, but they are also

321   active at low biomass concentrations and these loss terms are responsible for decreases in

322   biomass when growth conditions are unfavorable. Density-dependent losses are a

323   combination of grazing, viral attack, and aggregation and sinking following bloom collapse.

324   For each functional type, we distinguished between density-dependent feedback due to the

325   functional type's own biomass (α) and the feedback due to the aggregate biomass of all the

326   other functional types (ϕ). If the density-dependent loss terms are primarily due to grazing,

11

327   we could interpret α as representing losses due to grazers specializing on one functional

328   type and ϕ as representing losses due to generalist grazers supported by populations of the

329   other functional types. Since $\alpha < 0$ for all functional types, but ϕ is not different from 0 for

330   all types, the biomass of each functional type is largely regulated by specialist grazers and

331   generalist grazers have weak density-dependent effects.

332

333   *Species-level analysis*

334   Diatom species' net growth rates were smaller than the functional type counterpart

335   for all ten species examined (Fig. 3a). At the functional-type level, diatoms were weakly

336   affected by temperature ($\beta < 0.1$ week^{-1} °C^{-1}) and this result carried through for the diatom

337   species (most β^S close to 0.1, Fig. 3b). The optimal temperatures were extrapolated outside

338   the range of observed temperatures, and thus are very uncertain (data not shown). Diatom

339   species' half-saturation constants for irradiance are lower than the functional type

340   counterpart whereas diatom species' nitrogen half-saturation constants are higher than the

341   functional type level estimate.

342   For the species model, the density dependent loss analysis was redesigned to

343   identify species-specific density-dependent loss rates and generic functional type density-

344   dependent loss rates. The posterior distributions of the species-level density dependent

345   parameters α^S and ϕ^S imply a stronger negative feedback on each diatom species' biomass

346   growth from its own biomass than that from the combined biomass of other diatom species

347   i.e., $\alpha^s < \phi^s$ (Fig. 3e)^S), consistent with niche differentiation within functional types

348   (Mutshinda & O'Hara 2011). Some of the α^S and ϕ^S for diatoms were positive, suggesting

349   the presence of mutually beneficial or commensal effects in some species.

350

351   **Discussion**

352   Trait-based models of phytoplankton productivity promise to deliver robust

353   projections of phytoplankton community dynamics under future climate scenarios.

354   Phytoplankton traits are estimated in the lab one species at a time but are commonly

355   aggregated into functional types for ocean biogeochemical models (Anderson 2005, Le

356   Quéré et al. 2005, Litchman et al. 2006). There are several challenges that arise in the

357   estimates of phytoplankton traits for trait-based models. Most species in diverse

358   communities have not been systematically studied in the lab. Trait values vary across

359   species, even within functional types, and it is not clear how to produce an average trait

360   value for modeling functional types. In addition, there is considerable phenotypic plasticity

361   in traits. Furthermore, grazing rates, viral and parasitic loss rates, sinking rates and biotic

362   interactions, such as allelopathy or mutualisms, can be complex and highly variable from

363   species to species. It is difficult to get good estimates of loss terms, such as grazing rate and

364   viral lysis, that are inherently species specific and patchy in time and space, and we are just

365   starting to learn about the consequences of the many, complex biotic interactions between

366   phytoplankton and their microbial communities (Sher et al. 2011, Amin et al. 2015). It may

367   be possible to overcome some of these myriad challenges using phytoplankton traits

368   estimated directly from field data or by combining lab-based traits with niches estimated

369   from the field (Edwards 2016). Here we extract functional-type and species-level

370   phytoplankton traits from time-series data from a well-studied coastal temperate

371   phytoplankton community in the Western English Channel (Harris 2010, Widdicombe et al.

372   2010). While some of the traits estimated here are consistent with laboratory estimates of

373   similar traits on single species in the lab, many are not, indicating more work is needed to

374   understand how phytoplankton respond in natural communities.

375   Our estimates of maximum net growth rate for the phytoplankton functional types

376   range from 0.4 to 1.5 week^{-1} (a doubling time of 3.2 to 12 days) and for 10 individual

377   diatom species from 0.99 to 1.57 week^{-1} (a doubling time of 6.9 to 11 days). Our growth

378   rate estimates are considerably lower than lab-based estimates of growth rate from

379   unialgal cultures and *in situ* field estimates of growth rate of individual species (grazers

380   excluded) that can double more than once a day (Furnas 1990, 1991, Raven et al. 2005).

381   Maximum *in situ* growth rates for three of our ten diatom species have been estimated from

382   daily counts during April in the Irish Sea: *Pseudo-nitzchia* sp., 0.24 d^{-1}; *Guinardia delicatula*,

383   0.18 d^{-1}; *Lauderia annulata* 1.42 d^{-1}. These rates range from approximately the same to up

384   to 25 times our estimated maximum net growth rates (McKinney et al. 1997). Weekly

385   counts, used in our study, are likely to lead to smaller maximum net growth rates than daily

386   counts because the coupling between growth and loss processes will be tighter when

387   averaged over a week instead of a day. We expect our estimate of maximum growth rate to

388   be lower than traditional estimates of individual species growth rates in the lab and field

389   because our growth rate estimates include linear loss terms due to grazing, viral and

390   parasitic loss and are therefore similar to a net phytoplankton community growth rate.

391   Our values for net growth rate are consistent with satellite-based estimates of monthly

392   median phytoplankton growth rates in temperate regions with strong seasonal blooms,

393   0.35 to 4.2 week^{-1} (Westberry et al. 2008). Microzooplankton grazing at Station L4 and

394   elsewhere has been estimated to account for about two-thirds of phytoplankton growth

395   (Fileman et al. 2002, Calbet & Landry 2004, Chen et al. 2009, Bernard et al. 2012). Given

396   our estimates of maximum growth rates tend to be more than an order of magnitude lower

397   than estimates of growth rate from lab studies, this suggests loss rates due to grazing and

398   parasitoid and viral attack may be higher than often assumed.

399   It would be plausible for there to be no relationship between our field based

400   estimates of maximum growth rates across the functional types even if there are

401   differences in maximum net growth rate since the grazing and other linear loss terms

402   represent such a large fraction of maximum net growth rate. We find the rank order in our

403   estimates of net growth rates for the functional types (diatoms > dinoflagellates >

404   phytoflagellates > coccolithophorids) are generally consistent with growth rates reported

405   from laboratory culture work and field observations (Furnas 1991, Cermeño et al. 2005,

406   Raven et al. 2005, Laws 2013). In the Western English Channel we find diatoms have the

407   largest maximum net growth rate, which is roughly double that of coccolithophorids and

408   phytoflagellates (Fig. 2a). These results indicate that lab-based maximum growth rates

409   combined with a constant loss rate used by many models may be a reasonable proxy for net

410   growth rates in natural communities.

411   The effect of temperature on phytoplankton species growth rates is commonly

412   described using the Q_{10} approximation, which is the multiplicative effect of a 10°C change

413   in temperature on growth rate. This value is typically about 2, ranging from 1.88 to 2.3 for

414   phytoplankton (Eppley 1972, Bissinger et al. 2008). The range of temperatures at Station

415   L4 (about 8-18°C) is narrow compared to the width of many phytoplankton temperature

416   niches (Irwin et al. 2012, Boyd et al. 2013) so we used a linear model to describe the effect

417   of temperature on growth rate (see Montagnes et al. 2003 for additional rationale for using

418   a linear model). The temperature sensitivity of the functional types, β, is about 0.11 week^{-1}

419     $°C^{-1}$ for dinoflagellates, 0.06 week^{-1} $°C^{-1}$ for coccolithophorids and 0.05 week^{-1} $°C^{-1}$ for

420   diatoms, meaning that growth rate would increase from roughly 1 week^{-1} to 1.7 week^{-1} for

421   dinoflagellates, from 1 week^{-1} to 1.4 week^{-1} for coccolithophorids, and from 1 week^{-1} to 1.3

422   week^{-1} for diatoms with an increase in temperature of 6°C (half the annual amplitude in

423   temperature) starting below their temperature optimum (Fig. 2c). Analysis of the change in

424   maximum growth rate with temperature from unialgal lab cultures (Montagnes et al. 2003)

425   found a slope 0.11 to 0.54 week^{-1} $°C^{-1}$ for dinoflagellates, which is comparable to the

426   posterior means (0.11 week^{-1} $°C^{-1}$) found in this study (Fig. 2c), and 0.084 to 0.97 week^{-1} $°C^{-1}$

427   for diatoms which is higher than the posterior mean (0.055 week^{-1} $°C^{-1}$) found in this

428   study. For phytoflagellates our temperature trait β is 0.017 week^{-1} $°C^{-1}$ which is close to

429   zero and the credible interval is narrow and close to 0, so we conclude that temperature

430   has essentially no effect on the growth rate of this functional type at this site. Possible

431   interpretations for this result are that the phytoflagellates have broad temperature optima

432   for growth rate or the functional type is composed of many species with specialized

433   optimal growth temperatures spread across the range of observed temperatures (Eppley

434   1972, Boyd et al. 2013). This does not appear to be the case for dinoflagellates and

435   coccolithophorids; even if there is species turnover during the year, there is still a strong

436   imprint of temperature on the growth rate of the functional type as a whole. An alternative

437   explanation is that an increase in water column stability favors an increase in dinoflagellate

438   and coccolithophorid biomass accumulation (Margalef 1978, 1997). The optimal

439   temperature for growth at the functional type level varies as expected with diatoms and

440   phytoflagellates having lower optimal temperatures than dinoflagellates and

441   coccolithophorids, which bloom later in the season. Since temperature is correlated with

442   stability and we don't have an independent measure of stability, our model is unable to

443   distinguish between the direct effects of temperature and the effect of water column

444   stability on the growth rate of phytoplankton.

445   Temperature optima for individual diatom species were not identified within the

446   range of observed temperatures (not shown); we interpreted these results as consistent

447   with wide temperature response curves, relative to the narrow temperature range at

448   Station L4, for each species (Boyd et al. 2013). The estimates of the strength of the

449   temperature effect for individual diatom species ($β^S$, Fig. 3b) was roughly twice as high as

450   the effect on the diatom functional type. Averaging responses over many species in a

451   functional type could lead to weaker effects of temperature change as contrasting effects of

452   temperature on individual species partially cancel each other out.

453   Light and nutrient limitation of net growth rate is determined by Michaelis-Menten

454   half-saturation trait values, k_N and k_E. Three sources of inorganic nitrogen: nitrate, nitrite,

455   and ammonium are considered in our estimate of k_N for inorganic nitrogen. As a result our

456   estimate of k_N at the functional type level is largely determined by the inorganic nitrogen

457   species with the smallest half-saturation constant. Half-saturation constants for nitrogen

458   for phytoplankton species can vary from 0.08 to 8.4 μmol L^{-1} in the lab (Litchman et al.

459   2006). Our half-saturation constants for individual diatom species, many with large cell

460   size, ranged from 1.2-5 μmol L^{-1}, which is comfortably within this range. Our values for

461   functional types range from about 0.02 to 0.22 μmol L^{-1}, and are either on the lower end or

462   smaller than typical literature values for unialgal cultures. Diatoms and dinoflagellates as

463   functional types have k_N approximately a factor of ten smaller than many lab-based

464   literature estimates. The half-saturation constants for inorganic nitrogen for the

465   phytoplankton functional types at the site are also low relative to all but the lowest

466   nitrogen concentrations observed in seawater at this site (ranging from 0.1-16 μmol L^{-1},

467   only 10% of observations are less than 0.20 μmol L^{-1}), indicating that nitrogen limitation is

468   only a significant factor affecting growth rates of functional types, particularly diatoms and

469   dinoflagellates, in the warmest part of the summer. One reason k_N may be lower in the field

470   relative to laboratory studies is that organic nitrogen may be an important source of

471   nitrogen for some species, particularly the dinoflagellates and phytoflagellates, but also

472   some diatoms such as *Pseudo-nitzschia delicatissima* (Loureiro et al. 2009). If organic

473   sources are important for these groups, for example following the crash of a diatom bloom

474   when inorganic nitrogen concentrations are low, estimated k_N may be artificially low since

475   organic sources were not included in the model. Alternatively, since nitrogen is taken up

476   rapidly when available, bulk estimates of reactive nitrogen concentration sampled weekly

477   may be relatively uninformative at physiological scales (Laws 2013). The phytoflagellates

478   have the lowest k_N of approximately 0.02 μmol L^{-1}, which is less than half the value for

479   diatoms and roughly 10% of the value of coccolithophorids (Fig. 2d). The phytoflagellate

480   category is taxonomically diverse, but over half the biomass is found in unidentified cells

481   smaller than 5 μm in diameter. The resulting high surface area to volume ratio is consistent

482   with very low k_N (Fiksen et al. 2013). The most significant feature of our results is that the

483   phytoplankton dynamics at Station L4 is consistent with very low k_N compared to values

484   estimated from laboratory cultures (Litchman et al. 2007). The k_N at Station L4 are 5-10

485   fold smaller than half-saturation constants for nitrate often employed in ecosystem models

486   (Gregg et al. 2003, Merico et al. 2004). The intermediate complexity marine ecosystem

487   model constructed by Moore et al (2002) is an exception; this model uses a very low k_N for

488   ammonium of 0.004 μmol L^{-1} for small cells, much lower than our values for Station L4

489   (Moore et al. 2002). Generally k_N for ammonium are smaller than values for nitrate

490   (Litchman et al. 2007; Merico et al. 2004).

491   Light limitation is frequently parameterized by a half-saturation coefficient, k_E, or

492   the irradiance at which light saturates growth, E_k. For comparison between the two, we

493   divide E_k by 2 to roughly approximate k_E. In natural populations in coastal regions, E_k

494   varies from 40-500 μmol m^{-2} s^{-1} (Kirk 2010), corresponding to k_E of about 2-22 mol m^{-2} d^{-}

495   ^{1}. Estimates of k_E in unialgal cultures range from 3.5-7.8 mol m^{-2} d^{-1} (Litchman et al. 2006),

496   and varies with steady state irradiance (Gregg et al. 2003, Kirk 2010). At Station L4, our

497   values of k_E range from 8 to 20 mol m^{-2} d^{-1}, but these are based on sea-surface irradiance

498   and thus are larger than they would be based on average *in situ* irradiances. Individual

499   diatom species have k_E ranging from 6-14 mol m^{-2} d^{-1}, closer to the values for unialgal

500   cultures. These results suggest that irradiance at Station L4 is limiting for diatoms,

501   dinoflagellates and coccolithophorids during much of the year, since sea-surface PAR

502   ranges from 10-50 mol m^{-2} d^{-1} and only exceeds $E_k \cong 2k_E \cong 40$ mol m^{-2} d^{-1} for these groups

503   during short periods in the summer. By contrast, phytoflagellates have k_E near the

504   minimum levels of PAR and so they experience saturating irradiance for most of the year.

505   One possible hypothesis is that their small size confers a low pigment package effect,

506   meaning they have high light absorption per unit of pigment, giving them an advantage

507   over functional types with larger cells under low light conditions (Finkel & Irwin 2000,

508   Finkel 2001, Finkel et al. 2004). Furthermore, if some of the phytoflagellates use alternative

509   energy sources, they may require less chlorophyll and be less sensitive to changes

510   irradiance. While some dinoflagellates are known to be heterotrophic and mixotrophic

511   (Stoecker 1999), unlike phytoflagellates their growth rate is strongly affected by low

17

512   temperatures in winter, reducing their growth rate in winter relative to phytoflagellates

513   (Fig. 1). Phytoflagellates appear to be able to acclimate to very low light, giving them a

514   competitive advantage relative to the other functional types, especially in winter.

515   Many studies of zooplankton grazing focus on the linear grazing rate (Landry &

516   Hassett 1982, Calbet & Landry 2004, Zheng et al. 2015), which in our model is combined

517   with gross phytoplankton growth rate to obtain the maximum net growth rate trait, μ,

518   which is a constant for each phytoplankton functional type. More complex formulations of

519   zooplankton grazing rates permit diel and seasonal variation in grazing rates and non-

520   linear grazing rates (Tsai et al. 2005) or describe prey switching or selectivity by grazers

521   (Gentleman et al. 2003, Vallina et al. 2014), but we do not consider these mechanisms. Our

522   model incorporates density-dependent loss terms to describe consumption of

523   phytoplankton by grazers along with other loss processes. All four functional types exhibit

524   strong density-dependent loss. Assuming the loss term is primarily attributable to grazing,

525   diatoms and phytoflagellates are primarily grazed by specialists ($\alpha < 0$, Fig. 2) and

526   unaffected by generalist grazers ($\phi \cong 0$) while dinoflagellates and coccolithophorids were

527   roughly equally affected by specialist generalist grazers ($\phi \cong \alpha$). The difference between

528   specialist and generalist density-dependent losses is evidence of strong niche

529   differentiation for diatoms and phytoflagellates. The results at the species level are more

530   variable. Six of our ten diatom species exhibit positive density-dependent effects ($\phi^S > 0$,

531   Fig. 3c) with increased biomass of all other diatoms, which could be an indication that these

532   species experience less grazing pressure when the biomass of other diatoms is high ("kill

533   the winner") (Vallina et al 2014). Two species, *Guinardia delicatula* and *Pseudo-nitzschia*

534   *seriata*, have positive density-dependent effects resulting from their own biomass ($\alpha^S > 0$),

535   indicating that increases in their biomass can increase their own growth rates. Many

536   strains of *Pseudo-nitzschia* have been shown to produce the neurotoxin domoic acid (Bates

537   et al. 1998, Fehling et al. 2004), suggesting this positive density-dependence may be a

538   result of allelopathy, although *G. delicatula* does not produce toxins and *Pseudo-nitzschia*

539   *delicatissima* has $\alpha^S = 0$. Finally, three species have negative density dependence arising

540   from their own biomass ($\alpha^S < 0$). *Nitzschia closterium* is known to produce mucus that may

541   increase its export at high densities, which is consistent with this result (Najdek et al.

542   2005).

543   Our analysis of ten diatom species demonstrates the potential and challenges of this
544   approach for determining trait values and modeling dynamics of individual species. These
545   species were the most frequently observed in the population, but account for only 11% of
546   the total biomass, on average. Species with fewer observations are less likely to yield
547   informative estimates of trait values due to a lack of data, but account for the vast majority
548   of the biomass. Since our ten species sample is a minority component of the diatom
549   community and represents species present much of the year in contrast to species present
550   for only a few weeks at a time, there is no reason to expect the trait values of these species
551   to be representative of the functional type as a whole. In fact, we observed systematic
552   differences between trait values for these species and the diatom functional type:
553   maximum growth rate is lower and k_N is higher for the all the species analyzed relative to
554   the functional type. Even if we had a random sample of species with trait values
555   representative of the full distribution, determining functional-type level trait values by
556   averaging over species with different traits and changing contributions to the total
557   population can lead to errors due to Simpson's paradox (Chuang et al. 2009, Williams &
558   Hastings 2011). The uncertainties across the diatom species are large enough to suggest
559   that the trait values may be largely indistinguishable across many species (Fig. 3). An
560   independent analysis showed that diatoms species at Station L4 exhibit neutral dynamics
561   within the diatom functional type most of the time, indicating that predicting biomass
562   dynamics of individual species may be much harder than predicting the dynamics of the
563   aggregated biomass of a functional type (Mutshinda et al. 2016). While it is appealing to
564   estimate trait values for functional types from knowledge of individual species, it may be
565   more prudent to deemphasize species-level detail and use realized traits estimated from
566   biomass dynamics aggregated to the functional-type level.
567
568   **Conclusions**
569   This study enables a comparative analysis of trait values used in biogeochemical
570   models of phytoplankton communities and the trait values estimated from lab studies on
571   individual phytoplankton. The realized traits we quantified could be different from those
572   estimated in the lab because they are functional-type level aggregates and include factors
573   such as phenotypic plasticity and biotic interactions that may vary across species and

574   communities. At Station L4 in the Western English Channel, diatoms have the highest
575   maximum net growth rates, low half-saturation constant for nitrogen, a low temperature
576   optimum and low temperature sensitivity, and high specialist density-dependent loss rates.
577   By contrast, the dinoflagellates have intermediate maximum net growth rates, high
578   temperature optima and sensitivity. Coccolithophorids have the lowest maximum net
579   growth rate, high temperature optimum and intermediate temperature sensitivity, high
580   half-saturation constants for nitrogen and light, and like the dinoflagellates show similar
581   rates of specialist and generalist density-dependent losses. The phytoflagellates have low
582   maximum net growth rate, low optimum temperatures and sensitivities, low half-
583   saturation constants, and intermediate levels of specialist density-dependent losses. The
584   relative differences in maximum net growth rate, specifically the relatively high rates for
585   diatoms, are consistent with differences estimated in the lab and the field, but the absolute
586   magnitude of the rates are considerably lower because our maximum growth rates include
587   linear loss terms. A comparison of our results with traits estimated in the lab and used in
588   models yields a few insights. Grazing and other linear loss rates, as reflected in a reduction
589   of the gross growth rate, appear be even more important than usually appreciated. We see
590   evidence of complex biotic interactions that are difficult to assess in the lab: diatoms and
591   phytoflagellates are more susceptible to specialist loss rates, perhaps indicating specialist
592   grazers or viruses. At the species level, there appears to be evidence of species interactions
593   increasing the net growth rate of individual diatom species. The half-saturation constants
594   for nitrogen are considerably lower than typical lab estimates, consistent with the use of a
595   wide range of reactive nitrogen sources and widespread mixotrophy. There is considerable
596   variation in our estimates of the trait values within phytoplankton functional types, which
597   could be due to real physiological changes arising from acclimation to environmental
598   conditions over time, variation across species within a functional type, or a consequence of
599   insufficient data. Time-series of field data combined with our analysis gives us insight into
600   the mechanisms affecting the dynamics of species and whole functional types in natural
601   populations that may improve our ability to scale-up results from species-level studies in
602   the lab to community dynamics in the ocean.
603
604

614
615 **Figure 1.**

616 Observed (black line) and predicted (shaded region) $\log_{10}$ carbon biomass (mg C m^{-3}) of

617 each functional type (diatoms, dinoflagellates, coccolithophorids, and phytoflagellates) at

618 Station L4. The prediction region is the 95% credible range of biomass from the functional

619 type model.

620

Figure 1.

625
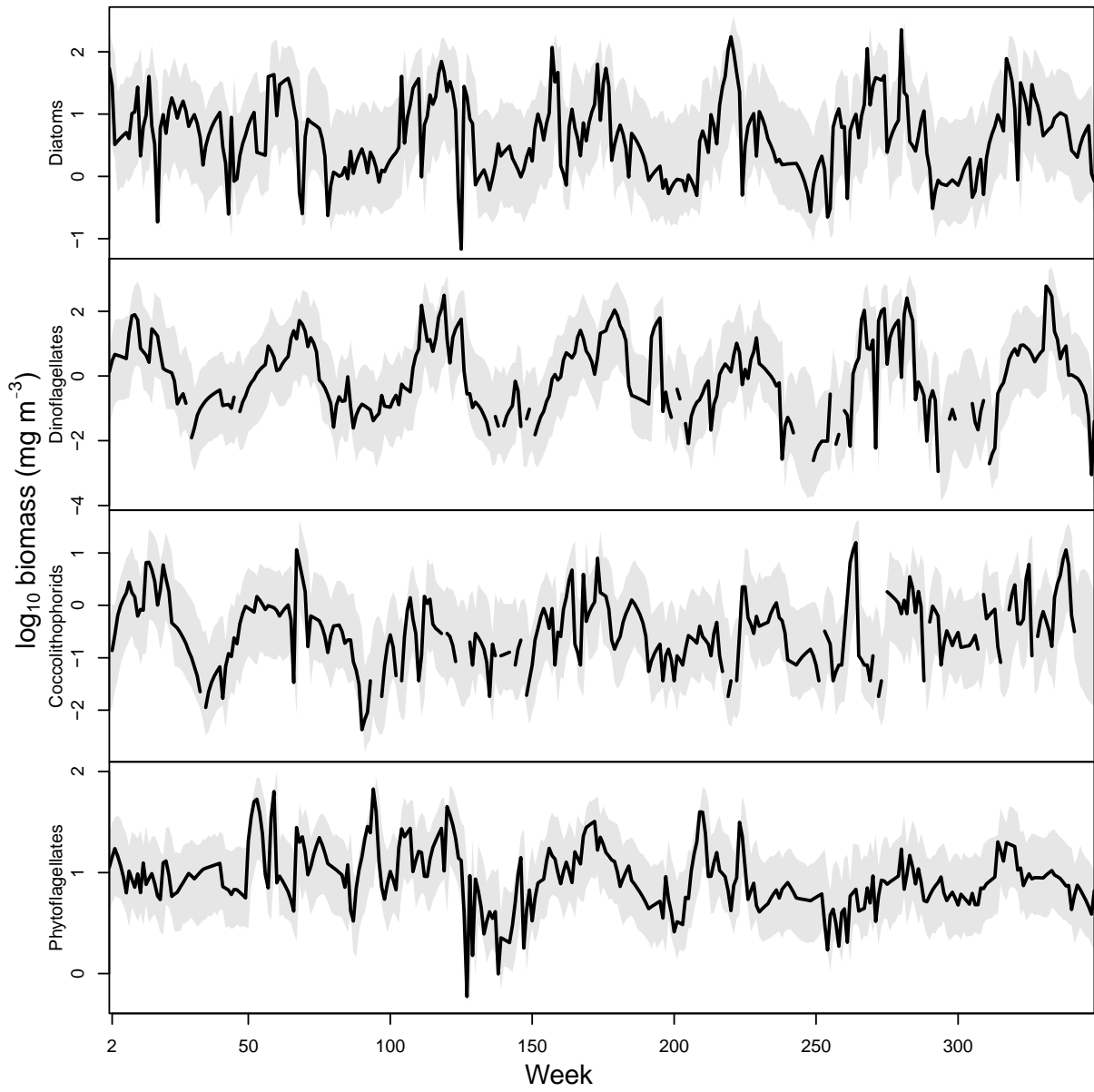
Figure 2.

Posterior distributions of traits governing growth rate at the functional type level. (a) Maximum net growth rate, μ (week^{-1}), (b) the optimal temperature θ (°C), (c) temperature sensitivity, β (week^{-1} °C^{-1}), (d) the half-saturation constants for nitrogen, k_N (µmol L^{-1}), (e) the half-saturation constants for irradiance, k_E (mol m^{-2} d^{-1}), and (f) density-dependent effects on the growth rate of each functional type attributed to their own biomass (α, solid circle) and to the total biomass of the other functional types in the community (ϕ, open circle). Box plots show median (thick line), the interquartile range (box) and the full range of the data or 1.5 times the interquartile range, whichever is smaller (whiskers). In panels (c) and (f) error bars indicate 95% credible intervals on the posterior means and are used because posterior distribution are approximately normal. In (f), the horizontal dashed line indicates no density-dependence. The vertical scale in (d) is logarithmic to facilitate the display of the wide range of values.

639
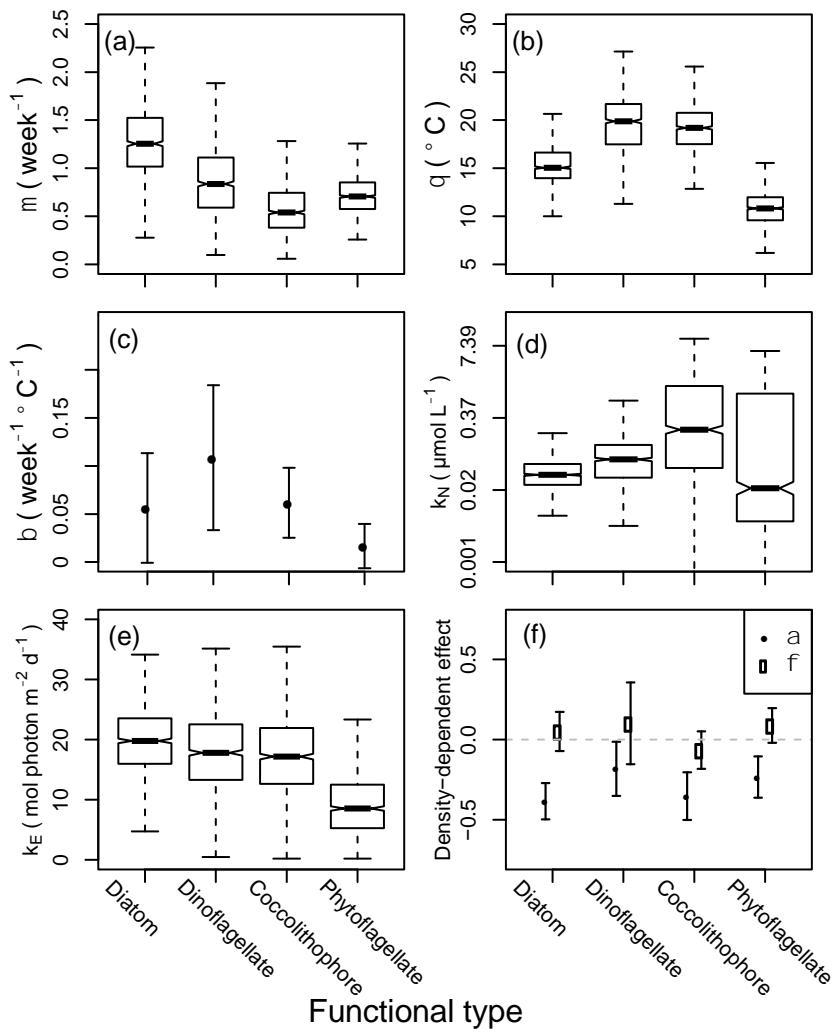
Figure 2.

Figure 3.

Species-level trait values for ten diatom species. Species are arranged in order of the number of weeks they are present in the time-series from *Nitzschia closterium* (93% of weeks) to *Lauderia annulata* (48%). (a) Maximum net growth rate, μ^S (week^{-1}), (b) temperature sensitivity, β^S (week^{-1} °C^{-1}), (c) the half-saturation constants for nitrogen, k_N^S (μmol L^{-1}), (d) the half-saturation constants for irradiance, k_E^S (mol m^{-2} d^{-1}), and (e) density-dependent effects on the growth rate of each functional type attributed to their own biomass (α^S, solid circle) and to the total biomass of the other functional types in the community (ϕ^S, open circle). Box plots show median (thick line), the interquartile range (box) and the full range of the data or 1.5 times the interquartile range, whichever is smaller (whiskers). In panels (b) and (e) error bars indicate 95% credible intervals on the posterior means and are used because posterior distribution are approximately normal. In (e), the horizontal dashed line indicates no density-dependence. The vertical scale in (c) is logarithmic to facilitate the display of the wide range of values.

658   **Figure 3.**

659
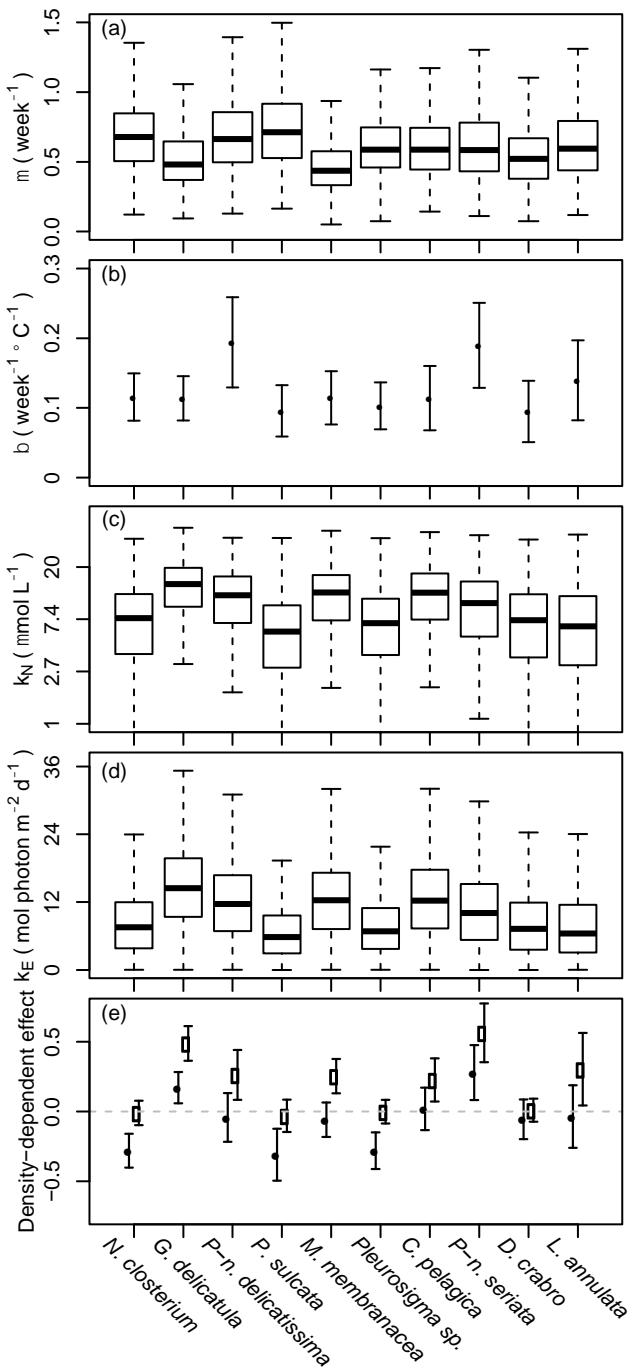
660

661 **Table 1.**

662 Key symbols for data and traits in the models. Traits for diatom species (as opposed to

663 functional types) have a superscript *S* added.

664

Symbol	Units	Interpretation
Y_i , y_i	mg C m^{-3}	Biomass, log biomass of functional types or species in week *i*
T_i	°C	Temperature in week *i*
N_i	mg N m^{-3}	Total inorganic N in week *i*
PAR$_i$	mol m^{-2} d^{-1}	Sea-surface irradiance in week *i*
μ, μ^S	week^{-1}	Maximum net growth rate for a functional type, species
r, *r*^{S}	week^{-1}	Realized net growth rate for a functional type, species
k_N, $k_N{}^S$	mg N m^{-3}	Half-saturation constant for growth as a function of N concentration
k_E, $k_E{}^S$	mol m^{-2} d^{-1}	Half-saturation constant for growth as a function of irradiance
β, β^S	week^{-1} °C^{-1}	Magnitude of linear increase in net growth rate with temperature, temperature sensitivity
θ, θ^S	°C	Temperature with maximum growth rate
α, α^S		Density dependent loss coefficient within functional type, diatom species
φ, φ^S		Density dependent loss coefficient due to other functional types, other diatom species

665

666

667

668 **Literature cited**

669 Amin S, Hmelo L, van Tol H, Durham B, Carlson L, Heal K, Morales R, Berthiaume C, Parker
670   M, Djunaedi B (2015) Interaction and signalling between a cosmopolitan
671   phytoplankton and associated bacteria. Nature 522:98-101
672 Anderson TR (2005) Plankton functional type modelling: running before we can walk? J
673   Plankton Res 27:1073-1081
674 Bates SS, Garrison DL, Horner RA (1998) Bloom dynamics and physiology of domoic-acid-
675   producing *Pseudo-nitzschia* species. NATO ASI series G ecological sciences 41:267-
676   292
677 Bernard KS, Steinberg DK, Schofield OM (2012) Summertime grazing impact of the
678   dominant macrozooplankton off the Western Antarctic Peninsula. Deep Sea
679   Research Part I: Oceanographic Research Papers 62:111-122
680 Bissinger JE, Montagnes DJS, Sharples J, Atkinson D (2008) Predicting marine
681   phytoplankton maximum growth rates from temperature: improving on the Eppley
682   curve using quantile regression. Limnol Oceanogr 53:487-493
683 Boyd PW, Rynearson TA, Armstrong EA, Fu F, Hayashi K, Hu Z, Hutchins DA, Kudela RM,
684   Litchman E, Mulholland MR (2013) Marine phytoplankton temperature versus
685   growth responses from polar to tropical waters–outcome of a scientific community-
686   wide study. Plos ONE 8:e63091
687 Calbet A, Landry MR (2004) Phytoplankton growth, microzooplankton grazing, and carbon
688   cycling in marine systems. Limnol Oceanogr 49:51-57
689 Cermeño P, Marañón E, Rodríguez J, Fernández E (2005) Large-sized phytoplankton
690   sustain higher carbon-specific photosynthesis than smaller cells in a coastal
691   eutrophic ecosystem. Mar Ecol Prog Ser 297:51-60
692 Chen B, Liu H, Landry MR, Dai M, Huang B, Sune J (2009) Close coupling between
693   phytoplankton growth and microzooplankton grazing in the western South China
694   Sea. Limnol Oceanogr 54:1084-1097
695 Chuang JS, Rivoire O, Leibler S (2009) Simpson's paradox in a synthetic microbial system.
696   Science 323:272-275
697 Colwell RK, Rangel TF (2009) Hutchinson's duality: the once and future niche. Proc Nat
698   Acad Sci 106:19651-19658
699 de Vargas C, Audic S, Henry N, Decelle J, Mahé F, Logares R, Lara E, Berney C, Le Bescot N,
700   Probert I, Carmichael M, Poulain J, Romac S, Colin S, Aury J-M, Bittner L, Chaffron S,
701   Dunthorn M, Engelen S, Flegontova O, Guidi L, Horák A, Jaillon O, Lima-Mendez G,
702   Lukeš J, Malviya S, Morard R, Mulot M, Scalco E, Siano R, Vincent F, Zingone A,
703   Dimier C, Picheral M, Searson S, Kandels-Lewis S, Coordinators TO, Acinas SG, Bork
704   P, Bowler C, Gorsky G, Grimsley N, Hingamp P, Iudicone D, Not F, Ogata H, Pesant S,
705   Raes J, Sieracki ME, Speich S, Stemmann L, Sunagawa S, Weissenbach J, Wincker P,
706   Karsenti E (2015) Eukaryotic plankton diversity in the sunlit ocean. Science
707   348:1261605
708 Denman KL, Peña MA (1999) A coupled 1-D biological/physical model of the northeast
709   subarctic Pacific Ocean with iron limitation. Deep-Sea Res Part II-Top Stud Oceanogr
710   46:2877-2908
711 Edwards KF (2016) Community trait structure in phytoplankton: seasonal dynamics from a
712   method for sparse trait data. Ecology. in press. doi: 10.1002/ecy.1581

713

714 Eppley RW (1972) Temperature and phytoplankton growth in the sea. Fish Bull 70:1063-
715   1085
716 Fehling J, Green DH, Davidson K, Bolch CJ, Bates SS (2004) Domoic acid production by
717   *Pseudo-nitzschia seriata* (Bacillariophyceae) in Scottish waters. J Phycol 40:622-630
718 Field C, Behrenfeld M, Randerson J, Falkowski P (1998) Primary production of the
719   biosphere: integrating terrestrial and oceanic components. Science 281:237-240
720 Fiksen Ø, Follows MJ, Aksnes DL (2013) Trait - based models of nutrient uptake in
721   microbes extend the Michaelis - Menten framework. Limnol Oceanogr 58:193-202
722 Fileman E, Cummings D, Llewellyn C (2002) Microplankton community structure and the
723   impact of microzooplankton grazing during an *Emiliania huxleyi* bloom, off the
724   Devon coast. Journal of the Marine Biological Association of the UK 82:359-368
725 Finkel ZV (2001) Light absorption and size scaling of light-limited metabolism in marine
726   diatoms. Limnol Oceanogr 46:86-94
727 Finkel ZV (2014) Marine Net Primary Production. Global Environmental Change. Springer
728 Finkel ZV, Beardall J, Flynn KJ, Quigg A, Rees TAV, Raven JA (2010) Phytoplankton in a
729   changing world: Cell size and elemental stoichiometry. J Plankton Res 32:119-137
730 Finkel ZV, Irwin AJ (2000) Modeling size-dependent photosynthesis: Light absorption and
731   the allometric rule. Journal of Theoretical Biology 204:361-369
732 Finkel ZV, Irwin AJ, Schofield O (2004) Resource limitation alters the 3/4 size scaling of
733   metabolic rates in phytoplankton. Mar Ecol Prog Ser 273:269-279
734 Flynn KJ, St John M, Raven JA, Skibinski DO, Allen JI, Mitra A, Hofmann EE (2015)
735   Acclimation, adaptation, traits and trade-offs in plankton functional type models:
736   reconciling terminology for biology and modelling. J Plankton Res 37:683-691
737 Furnas MJ (1990) In situ growth rates of marine phytoplankton: approaches to
738   measurement, community and species growth rates. J Plankton Res 12:1117-1151
739 Furnas MJ (1991) Net in situ growth rates of phytoplankton in an oligotrophic, tropical
740   shelf ecosystem. Limnol Oceanogr 36:13-29
741 Gelman A, Carlin JB, Stern HS, Dunson DB, Vehtari A, Rubin DB (2013) Bayesian data
742   analysis. Chapman and Hall, London, England
743 Gentleman W, Leising A, Frost B, Strom S, Murray J (2003) Functional responses for
744   zooplankton feeding on multiple resources: a review of assumptions and biological
745   dynamics. Deep Sea Research Part II: Topical Studies in Oceanography 50:2847-
746   2875
747 Gilks WR, Richardson S, Spiegelhalter DJ (1996) Markov Chain Monte Carlo in Practice.
748 Chapman & Hall, London, England.
749 Gilks WR (2005) Markov chain monte carlo. Wiley
750 Gregg WW, Ginoux P, Schopf PS, Casey NW (2003) Phytoplankton and iron: validation of a
751   global three-dimension ocean biogeochemical model. Deep-Sea Res II 50:3143-3169
752 Grover JP (1991) Non-steady state dynamics of algal population growth: experiments with
753   two chlorophytes. J Phycol 27:70-79
754 Harris R (2010) The L4 time-series: the first 20 years. J Plankton Res 32:577-583
755 Healey K, Monahan AH, Ianson D (2009) Perturbation dynamics of a planktonic ecosystem.
756   J Mar Res 67:637-666

757   Hood RR, Laws EA, Armstrong RA, Bates NR, Brown CW, Carlson CA, Chai F, Doney SC,
758   Falkowski PG, Feely RA, Friedrichs MAM, M.R. L, Moore JK, Nelson DM, Richardson
759   TL, Salihoglu B, Schartau M, Toole DA, Wiggert JD (2006) Pelagic functional group
760   modelling: progress, challenges and prospects. Deep-Sea Res II 53:459-512
761   Hutchinson GE (1957) Cold spring harbor symposium on quantitative biology. Concluding
762   remarks 22:415-427
763   Irwin AJ, Finkel ZV (2016) Phytoplankton functional types: a functional trait perspective.
764   In: Kirchman DM, Gasol JM (eds) Microbial ecology of the ocean. Wiley
765   Irwin AJ, Nelles AM, Finkel ZV (2012) Phytoplankton niches estimated from field data.
766   Limnol Oceanogr 57:787-797
767   Kirk JT (2010) Light and Photosynthesis in Aquatic Ecosystems. Cambridge University
768   Press
769   Landry M, Hassett R (1982) Estimating the grazing impact of marine micro-zooplankton.
770   Mar Biol 67:283-288
771   Laws EA (2013) Evaluation of in situ phytoplankton growth rates: a synthesis of data from
772   varied approaches. Annual review of marine science 5:247-268
773   Le Quéré C, Harrison SP, Colin Prentice I, Buitenhuis ET, Aumont O, Bopp L, Claustre H,
774   Cotrim Da Cunha L, Geider R, Giraud X (2005) Ecosystem dynamics based on
775   plankton functional types for global ocean biogeochemistry models. Global Change
776   Biology 11:2016-2040
777   Litchman E, Klausmeier CA, Miller JR, Schofield OM, Falkowksi PG (2006) Multi-nutrient,
778   multi-group model of present and future oceanic phytoplankton communities.
779   Biogeosciences 3:585-606
780   Litchman E, Klausmeier CA, Schofield OM, Falkowski PG (2007) The role of functional traits
781   and trade-offs in structuring phytoplankton communities: scaling from cellular to
782   ecosystem level. Ecology Letters 10:1-12
783   Lomas MW, Bonachela JA, Levin SA, Martiny AC 2014) Impact of ocean phytoplankton
784   diversity on phosphate uptake. Proc. Nat. Acad. Sci. USA 111: 17540-17545.
785   Loureiro S, Jauzein C, Garcés E, Collos Y, Camp J, Vaqué D (2009) The significance of organic
786   nutrients in the nutrition of Pseudo-nitzschia delicatissima (Bacillariophyceae). J
787   Plankton Res 31:399-410
788   MacArthur R (1960) On the relative abundance of species. Amer Natural 94:25-36
789   Margalef R (1978) Life-forms of phytoplankton as survival alternatives in an unstable
790   environment. Oceanol Acta 1:493-509
791   Margalef R (1997) Turbulence and marine life. Sci Mar Suppl 1 61:109-123
792   McKinney E, Gibson C, Stewart B (1997) Planktonic diatoms in the North-West Irish Sea: a
793   study by automatic sampler. Biology and Environment: Proceedings of the Royal
794   Irish Academy. Royal Irish Academy
795   Menden-Deuer S, Lessard EJ (2000) Carbon to volume relationships for dinoflagellates,
796   diatoms, and other protist plankton. Limnology & Oceanography 45:569-579
797   Merico A, Tyrrell T, Lessard EJ, Oguz T, Stabeno PJ, Zeeman SI, Whitledge TE (2004)
798   Modelling phytoplankton succession on the Bering Sea shelf: role of climate
799   influences and trophic interactions in generating Emiliania huxleyi blooms 1997–
800   2000. Deep Sea Research Part I: Oceanographic Research Papers 51:1803-1826
801   Montagnes DJS, Kimmance SA, Atkinson D (2003) Using Q_{10}: Can growth rates increase
802   linearly with temperature? Aquatic Microbial Ecology 32:307-313

803   Moore JK, Doney SC, Kleypas JA, Glover DM, Fung IY (2002) An intermediate complexity
804   marine ecosystem model for the global domain. Deep-Sea Res II 49:403-462
805   Mutshinda CM, Finkel ZV, Widdicombe CE, Irwin AJ (2016) Ecological equivalence of
806   species within phytoplankton functional groups. Funct Ecol:in press
807   Mutshinda CM, O'Hara RB, Woiwod IP (2009) What drives community dynamics?
808   Proceedings of the Royal Society of London B: Biological Sciences 276:2923-2929
809   Mutshinda CM, O'Hara RB, Woiwod IP (2011) A multispecies perspective on ecological
810   impacts of climatic forcing. J Animal Ecol 80:101-107
811   Mutshinda CM, O'Hara, RB (2011) Integrating the niche and neutral perspectives on
812   community structure and dynamics. Oecologia 166: 241-251.
813   Najdek M, Blažina M, Djakovac T, Kraus R (2005) The role of the diatom *Cylindrotheca*
814   *closterium* in a mucilage event in the northern Adriatic Sea: coupling with high
815   salinity water intrusions. J Plankton Res 27:851-862
816   R Core Team (2016) R: A language and environment for statistical computing. R
817   Foundation for Statistical Computing, Vienna, Austria
818   Raven J, Finkel Z, Irwin A (2005) Picophytoplankton: Bottom-up and top-down controls on
819   ecology and evolution. VIE ET MILIEU-LIFE AND ENVIRONMENT 55:209-215
820   Raven JA (2011) The cost of photinhibition. Physiol Plant 142:87-104
821   Saitoh T, Chr N, Bjornstad ON (1997) Density dependence in fluctuating grey-sided vole
822   populations. J Animal Ecol:14-24
823   Sher D, Thompson JW, Kashtan N, Croal L, Chisholm SW (2011) Response of
824   *Prochlorococcus* ecotypes to co-culture with diverse marine bacteria. The ISME
825   Journal 5:1125-1132
826   Sournia A, Chretiennot-Dinet M-J, Ricard M (1991) Marine phytoplankton: how many
827   species in the world ocean? J Plankton Res 13:1093-1099
828   Stoecker DK (1999) Mixotrophy among dinoflagellates. Journal of Eukaryotic Microbiology
829   46:397-401
830   Sugihara G (1980) Minimal community structure: an explanation of species abundance
831   patterns. Am Nat 116:770-787
832   Thomas A, O'Hara B, Ligges U, Sturtz S (2006) Making BUGS open. R news 6:12-17
833   Tsai A-Y, Chiang K-P, Chang J, Gong G-C (2005) Seasonal diel variations of picoplankton and
834   nanoplankton in a subtropical western Pacific coastal ecosystem. Limnol Oceanogr
835   50:1221-1231
836   Vallina SM, Ward B, Dutkiewicz S, Follows M (2014) Maximal feeding with active prey-
837   switching: A kill-the-winner functional response and its effect on global diversity
838   and biogeography. Prog Oceanogr 120:93-109
839   van der Ploeg RR, Kirkham M (1999) On the origin of the theory of mineral nutrition of
840   plants and the law of the minimum. Soil Sci Soc Am J 63:1055-1062
841   Westberry TK, Behrenfeld MJ, Siegel DA, Boss E (2008) Carbon-based primary productivity
842   modeling with vertically resolved photoacclimation. Global Biogeochem Cycles 22:1-
843   18
844   Widdicombe C, Eloire D, Harbour D, Harris R, Somerfield P (2010) Long-term
845   phytoplankton community dynamics in the Western English Channel. J Plankton Res
846   32:643-655

847   Williams PD, Hastings A (2011) Paradoxical persistence through mixed-system dynamics:
848   towards a unified perspective of reversal behaviours in evolutionary ecology.
849   Proceedings of the Royal Society of London B: Biological Sciences 278:1281-1290
850   Zheng L, Chen B, Liu X, Huang B, Liu H, Song S (2015) Seasonal variations in the effect of
851   microzooplankton grazing on phytoplankton in the East China Sea. Contin Shelf Res
852   111:304-315
853
854